density allows for porosities ranging from 0 to about 60%. Our current estimate of the density of Eros (2.5 ± 0.8 g/cm^3) is indistinguishable from that of 243 Ida (2.6 ± 0.5 g/cm^3), the only other S-type asteroid for which a mass and density have been determined (*12*).

Small asteroids such as Eros are expected to be either collisional fragments of larger precursor bodies or accumulations of discrete fragments ("rubble piles") (*13*). However, the presence of a linear marking running at least 20 km across the asteroid (Fig. 4) implies that Eros may be structurally continuous. High-resolution views expected during the orbital phase of the mission should reveal whether this apparent linear marking is a ridge, a fault, an exposed layer, or a series of aligned structures.

Five craters can be identified in the images; the two largest, 8.5 and 6.5 km across, have sizes consistent with the maximum crater diameter expected on a body with the dimensions of Eros (*14*). Contrary to the situation observed by NEAR on C-type asteroid Mathilde (*11*), the outlines of Eros are not dominated by a high spatial density of large craters (*10*). The number of craters identified suggests that Eros has a crater density intermediate between the low density of craters observed on asteroid 951 Gaspra and the saturated surface of Ida (*15*). If so, the finding could indicate that Eros is comparatively young, resulting from the disruption of a precursor parent body relatively recently, with insufficient time for its surface to have become saturated with craters once more. Alternatively, the finding could indicate that the cratering record was reset during the formation of one of the large craters. If the detailed measurements expected from the orbital phase of NEAR confirm the suggestion that Eros is a relatively low-porosity body with significant structural continuity, then Eros would be similar to S-type asteroid Gaspra (*16*). NIS spectra show broad similarity to telescopic data (*20*), including evidence for 1- and 2-μm bands. Both features are indicative of pyroxene or olivine, or both.

References and Notes

1. R. W. Farquhar *et al.*, *J. Astronaut. Sci.* **43**, 353 (1995).
2. D. K. Yeomans *et al.*, *Science* **285**, 560 (1999).
3. D. K. Yeomans, *J. Astronaut. Sci.* **43**, 417 (1995); S. J. Ostro *et al.*, *Icarus* **84**, 334 (1990); D. Mitchell *et al.*, *ibid.* **131**, 4 (1998); M. D. Hicks *et al.*, *ibid.*, in press.
4. The sequence began with an inbound satellite search at 15:30 UTC when the spacecraft was 11,672 km from Eros and the solar phase angle was 84°. Near closest approach (3827 km), the goal was to obtain continuous coverage of Eros. Because of uncertainties in the asteroid's position relative to the spacecraft, a large area of the sky had to be imaged to ensure that views of Eros were obtained near closest approach. A sequence was designed that interlaced 2 × 2 mosaics (2 frames across and 2 down) with an additional single frame centered on the most probable position of Eros. Images were taken through seven filters at each position with automatic exposure (*19*). At closest approach, a single 4 × 4 clear-filter mosaic sequence was executed.
5. J. Warren *et al.*, *Space Sci. Rev.* **82**, 101 (1997).
6. During an attitude anomaly that occurred immediately after the aborted burn on 20 December and persisted for 27 hours, more than 28 kg of hydrazine was burned by attitude control jets, creating a diffuse cloud of hydrazine and burn products around the spacecraft. We believe that the enhanced scattering in the Eros flyby images resulted when these materials condensed on the cold outer optics of the imager. Observations of star fields are planned during the remainder of the cruise to Eros to monitor the light-scattering and transmission properties of the camera.
7. Our estimate is based on P. D. Hamilton and J. A. Burns, *Icarus* **92**, 118 (1991).
8. D. Mitchell *et al.*, *ibid.* **131**, 4 (1998).
9. B. Zellner, *ibid.* **28**, 149 (1976).
10. J. Veverka *et al.*, *Science* **278**, 2109 (1997); D. K. Yeomans *et al.*, *ibid.*, p. 2106.
11. S-type asteroids have moderate albedos and spectra, indicating silicates such as olivine or pyroxene. C-type asteroids have low albedos and spectra, indicating carbon or carbonaceous materials on their surfaces [for example, D. J. Tholen and M. A. Barucci, in *Asteroids II*, R. P. Binzel, T. Gehrels, M. S. Matthews, Eds. (Univ. of Arizona Press, Tucson, AZ, 1989), pp. 298–315].
12. M. J. S. Belton *et al.*, *Nature* **374**, 785 (1995).
13. H. Melosh and E. Ryan, *Icarus* **129**, 562 (1997).
14. S. K. Croft, *ibid.* **99**, 402 (1992).
15. For Gaspra, see C. R. Chapman *et al.*, *ibid.* **120**, 231 (1996). For Ida, see C. R. Chapman *et al.*, *ibid.*, p. 77.
16. On the surface of Gaspra, Galileo observed structures of global dimensions (such as planar facets and linear grooves). We note that the specific predictions about the shape of Eros made recently by W. F. Bottke *et al.* (*Astron. J.*, in press) are not supported by the NEAR images. That model considers Eros to be a rubble pile, the shape of which has been influenced by tidal forces during a presumed close passage to Earth.
17. J. Veverka *et al.*, *Icarus* **107**, 72 (1994).
18. For Dactyl, see C. R. Chapman *et al.*, *Nature* **374**, 783 (1995); M. Belton *et al.*, *Icarus* **120**, 1 (1996). For the discovery of Eugenia's moon, see W. J. Merline *et al.*, *Nature*, in press.
19. The MSI camera covers the spectral range from 400 to 1100 nm. For filter specification and nomenclature, see J. Veverka *et al.*, *J. Geophys. Res.* **102**, 23709 (1997). The MSI automatic exposure algorithm is described by S. E. Hawkins *et al.* [*Space Sci. Rev.* **82**, 31 (1997)].
20. S. Murchie and C. Pieters, *J. Geophys. Res.* **101**, 2201 (1996).
21. M. D. Hicks *et al.*, *Icarus*, in press.
22. We thank the Mission Design, Mission Operations, and Spacecraft teams of the NEAR Project at the Applied Physics Laboratory of Johns Hopkins University for their dedicated and vigorous efforts that led to the successful return of key data from the 23 December 1998 flyby. We thank three anonymous reviewers for their comments and suggestions.

16 March 1999; accepted 1 June 1999

Pacemaking the Ice Ages by Frequency Modulation of Earth's Orbital Eccentricity

J. A. Rial

Evidence from power spectra of deep-sea oxygen isotope time series suggests that the climate system of Earth responds nonlinearly to astronomical forcing by frequency modulating eccentricity-related variations in insolation. With the help of a simple model, it is shown that frequency modulation of the approximate 100,000-year eccentricity cycles by the 413,000-year component accounts for the variable duration of the ice ages, the multiple-peak character of the time series spectra, and the notorious absence of significant spectral amplitude at the 413,000-year period. The observed spectra are consistent with the classic Milankovitch theories of insolation, so that climate forcing by 100,000-year variations in orbital inclination that cause periodic dust accretion appear unnecessary.

Understanding the climate of the recent geological past is of importance, because finding out how Earth's environment has transformed the heat input from the sun into climate variations can help predict future global climate change. Most of our knowledge about climatic variations in the Plio-Pleistocene (the last 5.2 million years) is extracted from time series of oxygen isotope ratios, a proxy for global ice volume generally known as the δ^{18}O records (Fig. 1A). The records show that during the last million years, Earth has experienced at least 10 major glaciations, which according to the astronomical theory of the ice ages (*1*) are the consequence of secular variations in insolation caused by changes in Earth's orbital eccentricity, axial tilt, and longitude of perihelion (Earth's closest approach to the sun). The theory finds support in the fact that the spectra of the δ^{18}O records contain some of the same frequencies as the astronomical variations (*2–4*), but a satisfactory explanation of how the changes in orbital eccentricity are transformed into the ~100-ky (1 ky = 1000 years) quasi-periodic fluctuations in global ice volume indicated by the data has not yet been found (*5*).

For instance, a fundamental difficulty is to understand the notable absence in the δ^{18}O data of a significant response to the 413-ky component of the orbital eccentricity, whose signal power is of the same order of magnitude as the 95-ky component. This has been called the "400-ky problem" by Imbrie and Imbrie (*6*).

Department of Geological Sciences, and Wave Propagation Laboratory, University of North Carolina at Chapel Hill, Chapel Hill, NC 27599–3315, USA. E-mail: jar@email.unc.edu

One of the well-known features of the $\delta^{18}O$ time series from deep-sea sediments is the slight but evident change in the duration of consecutive glacial periods (7), which oscillates from about 120 to 80 ky. For instance, the interval between the last two interglacials is 120 ky, while 400 thousand years ago (ka) the interglacial interval was nearly 80 ky, with three successive interglacials occurring in less than 200 ky. This is reflected clearly in the spectrogram of Fig. 1B (moving window Fourier transform) of Ocean Drilling Program (ODP) Site 806 (8), a representative paleoclimate record. The power of the eccentricity band (~0.01 cycles/ky) in the spectrogram occurs along an approximately sinusoidal curve (as indicated by the dashed curve overlay), apparently because of periodic switching of main power from ~120 ky to ~80 ky every 400 ky or so. This fact suggests frequency modulation (FM) of the ~100-ky eccentricity signals by the longer-period, 413-ky component. Such frequency modulation is entirely similar to electronic modulation of a high-frequency carrier by a low-frequency modulating signal, as used in FM radio and television broadcasting (9).

In addition to the characteristic sinusoidal shape of the spectrogram, frequency modulation of a single frequency carrier widens the spectral band by the addition of sidebands. Sidebands are spectral peaks distributed symmetrically on both sides of a carrier's peak at intervals equal to integer multiples of the modulating frequency (10). The appearance of orderly distributed sidebands in the power spectra of all the $\delta^{18}O$ data analyzed here further supports the presence of frequency modulation. For

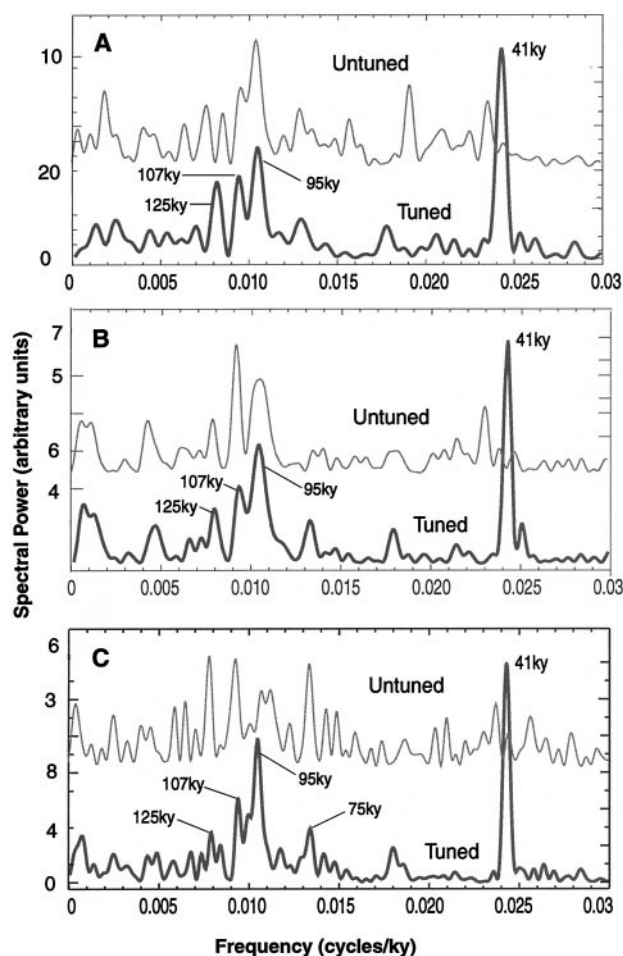**Fig. 2.** The multiple-peak character of the $\delta^{18}O$ spectra is common to both the orbitally tuned and orbitally untuned records. Orbital tuning may, however, change the relative amplitudes of some peaks, as shown in (C). Modeling these differences provides further support for the FM hypothesis. The strong 41-ky peak in the orbitally tuned spectra is caused by tuning at that frequency. Data are from ODP Site 677 (A), Site 846 (B), and Site 849 (C). Bandwidths are 0.0011 ky^{-1} (A), 0.0014 ky^{-1} (B), and 0.00093 ky^{-1} (C). Age models are described in (13).
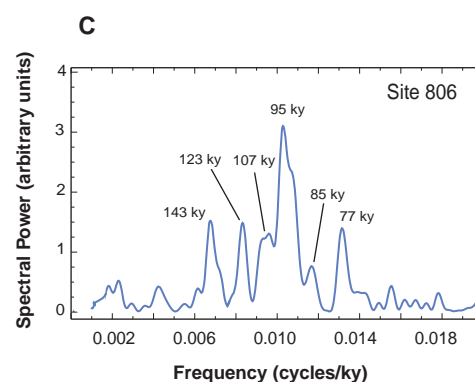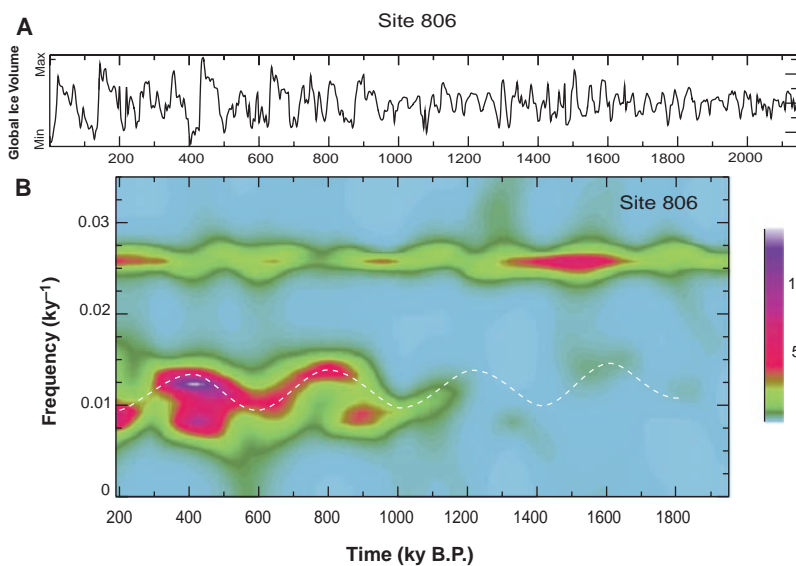

Fig. 1. (**A**) Oxygen isotope time series from ODP Site 806 shows the fluctuations in ice volume over the last 2.1 million years. (**B**) Time-frequency spectrogram showing the distribution of signal power in the isotope record. The horizontal band around 0.025 cycles/ky is the linear, single-frequency, time-invariant response of the climate system to the 41-ky variation in axial tilt, enhanced by orbital tuning. The much wider band of power centered at 0.01 cycles/ky is the response to variations in orbital eccentricity. In sharp contrast to the response to axial tilt, this is an age- and frequency-dependent response, likely to be nonlinear. The dashed sinusoid overlay indicates that the response appears to switch from one predominant low frequency to a predominant high frequency in cycles of ~413 ky (the period of the sinusoid), strongly suggesting the presence of frequency modulation (FM). The spectrogram is computed with 350-ky-long windows for the Fast Fourier Transform and 10-ky lag between overlapping windows. (**C**) Around the 95-ky eccentricity component the power spectrum shows a characteristic multi-peaked power distribution that can be easily predicted assuming a 95-ky "carrier" frequency-modulated by a 413-ky modulating signal and a 826-ky subharmonic. The positions of the peaks are essentially insensitive to orbital tuning of the original time series.

Fig. 3. The effect of time window length is crucial to the interpretation of power spectra of long-period δ¹⁸O data. Time windows here are (**A**) 0 to 2140 ky B.P., (**B**) 0 to 1070 ky B.P., and (**C**) 0 to 600 ky B.P. From (A) to (C), the spectra depict the strong loss in resolution when the δ¹⁸O time window is shorter than about 1000 ky. As shown, the worst spectral resolution occurs for a 600-ky window (C), which obscures the multiple-peak character of the spectrum. Both tuned and untuned records were studied, and identical loss of resolution and a similar single peak at 100 ky emerges when the short 600-ky-long window is used in both. This short window length was used, however, by Muller and Mac-Donald (*14*) to determine the power spectra of nine δ¹⁸O records, all of which look very much like (C) above (Fig. 3) (*14*), a feature which they interpreted as an indication of climate forcing by 100-ky oscillations of Earth's orbital plane. Bandwidths are 0.00093 ky⁻¹ (A), 0.0019 ky⁻¹ (B) and 0.0033 ky⁻¹ (C). The data for Site 849 is from (*18*).
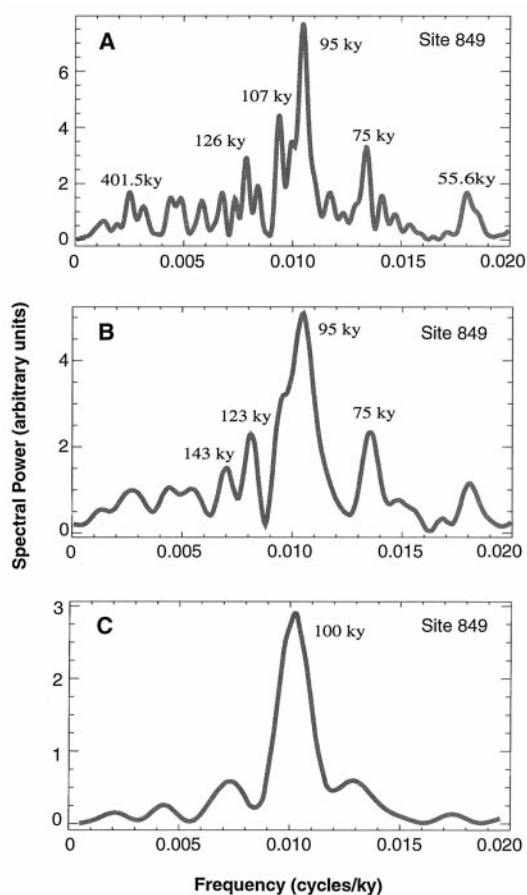

Fig. 4. (**A**) High resolution spectra (signal bandwidth 0.00093 cycles/ky) of the tuned Site 849 record (see Fig. 3) is shown compared to the Fourier transform of the model FM signal given by Eq. 3. As predicted by FM theory, the modulating power does not appear as a spectral peak, but as separation between each carrier and its sidebands. (**B**) High-resolution spectra (signal bandwidth 0.00093 cycles/ky) of the untuned Site 849 record. The comparison is made again with the Fourier transform of the model signal in Eq. 3. In order to optimize the fit, the modulating parameters ε and ε' need to be increased by 20%. This suggests stronger modulation intensity, which causes the peak of the 95-ky carrier to be reduced in size relative to the sidebands, as predicted by FM theory. Thus, the FM mechanism appears robust for the untuned record. All the peaks predicted by the FM theory are present in both the tuned and the untuned spectra. A 95% confidence interval of 0.0005 cycles/ky was calculated from the mismatch between model peaks and the observed spectra. This is about 40% of the sideband separation of 1/826 ky⁻¹.
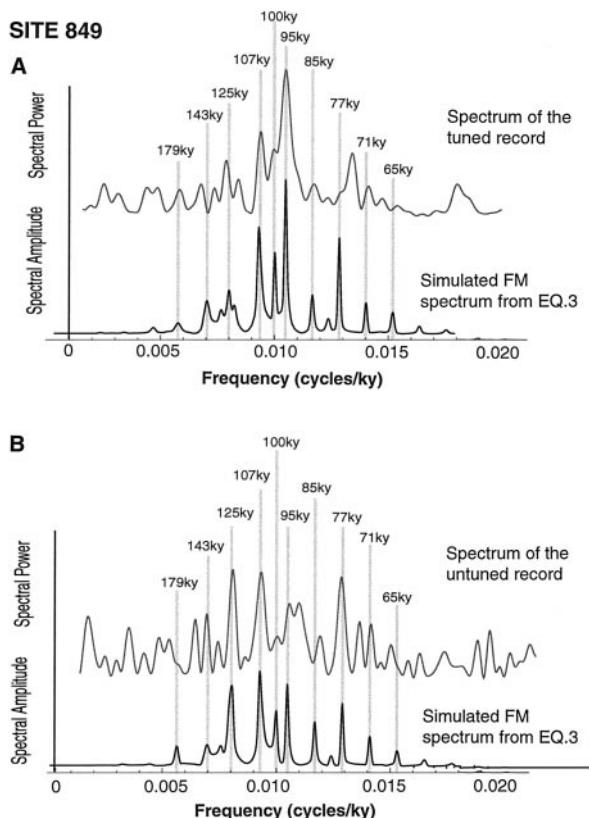
instance, the power spectrum of Site 806 (Fig. 1C) shows evidence of frequency modulation as the observed 75- and 123-ky peaks coincide with the predicted sidebands of a 95-ky carrier frequency-modulated by a 413-ky signal, and the 85-, 107-, and 143-ky peaks coincide with the predicted sidebands of a 95-ky carrier frequency-modulated by the 826-ky subharmonic of the 413-ky signal (*11*).

Another important prediction of the FM hypothesis is that the power spectrum of an FM signal does not contain the modulating signal as a spectral peak, but as the separation interval between sidebands (*9*), a fact that is entirely consistent with the well-known absence of a distinctive 413-ky spectral peak in paleoclimate data.

It is important to point out that the spectra in Fig. 1 are obtained from an orbitally tuned (*12*) time series. Orbital tuning is routinely applied to raw δ¹⁸O time series in order to establish a common time scale for all records regardless of location and sedimentation rate differences. However, the "clock" used to develop the chronology is the rhythm of any of the orbital periodicities, including eccentricity. Hence, it is possible that orbital tuning introduces bias or even spectral peaks not present in the data, and thus it is useful and prudent to analyze and compare both tuned and untuned records. In their original form the orbitally untuned records are of δ¹⁸O variation versus depth; the depth scale is converted to time using known published ages (determined by biostratigraphic or magnetic methods, or both) at one or two anchor points (*13*), and assuming a constant sedimentation rate for the rest of the sediment core. In spite of its obvious drawbacks, this assumption produces spectra similar enough to the tuned data to permit easy cross-identification of spectral peaks. As shown in Figs. 2 through 4, sidebands separated from the main spectral power as predicted by the FM hypothesis are a common feature in both tuned and untuned spectra from different sites, and as discussed below (Fig. 4), the effect of tuning appears to reduce, rather than to increase, the number of recognizable spectral peaks in the eccentricity band.

Since what follows hinges on the interpretation of power spectra, it is important to note that because of the strong age dependence of the eccentricity band (Fig. 1B), resolving individual spectral peaks depends critically on the window length chosen to calculate the spectrum. This becomes an important issue, because the apparent presence of a single power peak at 100 ky (Fig. 3) in several δ¹⁸O recordings has been interpreted as due to variations in Earth's orbital inclination, which force the planet to periodically cross a ring of extraterrestrial dust, thus causing the ice ages of the last million years (*14*). This conclusion is, however, based on power spectra computed from time windows spanning just the last 600 ky, an interval half the duration of typical eccentricity signals, which have sig-

nificant power from 0 to about 1200 ka (Fig. 1B). As shown in Fig. 3, a 600-ky window limits the resolving power in the eccentricity band so much that important details are lost, and it is thus plausible that the presence of the 100-ky single spectral peak is due simply to merging of the 95-, 107-, and 125-ky eccentricity-related spectral peaks because the time window is too short, rather than from periodic changes in orbital inclination (*15, 16*).

If frequency modulation indeed occurs, it should be possible to replicate the observed variation in ice age duration seen in the $\delta^{18}O$ records using an appropriate FM formula. A simple mathematical form of a frequency-modulated signal is

$$\sin[\Omega t + \varepsilon \sin (\omega t)] \qquad (1)$$

where $\Omega = 2\pi f_c$, $\omega = 2\pi f_m$ and f_c and f_m are the frequencies of the carrier and the modulating signals respectively, $\varepsilon = \Delta f_c/f_m$ is the modulation index (*17*), and Δf_c is the frequency deviation, a measure of the bandwidth produced by the modulation (*9, 10*). Since the predominant frequency shifts from ~120 to ~80 ky, which is also the observed shift in ice age duration, $\varepsilon \approx 0.7$ (moderate modulation) for $f_m = 1/413$ cycle/ky.

Trigonometric functions of the form in Eq. 1 can be represented by an infinite series of Bessel functions of increasing order, such as

$$\sin[\Omega t + \varepsilon \sin(\omega t)] = J_0(\varepsilon) \sin\Omega t$$

$$+ \sum_{n=1}^{\infty} J_n(\varepsilon) [\sin(\Omega + n\omega)t$$

$$+ (-1)^n\sin(\Omega - n\omega)t] \qquad (2)$$

which clearly indicates that the Fourier spectrum of a FM signal such as given by Eq. 1 is composed of a central spectral peak at the carrier frequency f_c and additional spectral peaks (sidebands) at the frequencies $f_c \pm nf_m$ for $n = 1, 2, 3 \ldots$, so that the modulating frequency $f_m = \omega/2\pi$ appears in the power spectrum only as the interval between spectral peaks, but not as a spectral peak itself (*9*). A plausible model to simulate the $\delta^{18}O$ records should thus contain the 125-, 100-, and 95-ky harmonics as carrier signals and the 413-ky and, as explained below, a 826-ky subharmonic as the modulating signals. The following model is possibly the simplest

$$\Phi_{FM}(t) = a \sin[2\pi t/95 + \varepsilon \sin(2\pi t/413)$$
$$+ \varepsilon' \sin(2\pi t/826)]$$
$$+ b \sin[2\pi t/100 + \varepsilon \sin(2\pi t/413)]$$
$$+ c \sin[2\pi t/125 + \varepsilon \sin(2\pi t/413)] \quad (3)$$

where t is the time in kiloyears. The constants a through c are adjustable parameters, with a typically three times greater than b or c, reflecting the relative strength of the eccentricty com-

ponents. The term ε' is the modulating index for the subharmonic, and since $\varepsilon \sim 1$ then $\varepsilon' \sim 2$, since f_m is halved. In spite of the simplicity of Eq. 3, its spectrum (Fig. 4), reproduces every spectral peak in the power spectra of the tuned and untuned records, including the prominent combination tone at 107 ky (Figs. 2 and 4) which occurs only if the additional modulation by a 826-ky subharmonic is included in the model, as in Eq. 3. Frequency modulation as described by Eq. 3 is nonlinear in the sense that the effect produced by two modulating frequencies is not equal to the sum of the signals produced separately by each (*18*).

The 107-ky spectral peak is here interpreted as a combination tone (1/107 = 1/95 − 1/826) produced by nonlinear response of the climate system. Although the precise mechanism by which this may occur in the real climate system is not resolved here, an explanation is attempted below. On the other hand, Eq. 3 uses superposition of each modulated carrier to construct the total signal, and so in this sense the response is assumed linear.

Figure 4 shows that even when a spectrum is distorted by tuning, the sidebands can still be identified and the general structure of the spectrum understood. The distortion occurs because tuning in this case targeted the eccentricity frequencies (*19*), thus enhancing the amplitude of the 95-ky eccentricity carrier to the expense of its sidebands, as becomes apparent when comparing Fig. 4B with Fig. 4A. Accordingly, to compensate for tuning and simulate the untuned spectra required just a 20% increase in ε' in Eq. 3.

It should be noted that the model spectra shown in Fig. 4 account not only for all the periods present, but also for those not present.

As mentioned before, FM theory predicts that the modulating frequencies appear only as intervals between sidebands, and not as spectral peaks. Hence, if the role of the 413-ky eccentricity component is indeed to frequency-modulate the higher frequency components, we can expect to find signal power at 413 ky in all the $\delta^{18}O$ records, though not in the form of a spectral peak, but rather as the interval between sidebands (clear examples are Figs. 1C, 3A, and 4). Thus, the apparent absence of a 413-ky spectral peak in Earth's climate response, also known as "the 400-ky problem" (*6*), may not be a problem after all, but the logical consequence of the fact that the 1/413 ky^{-1} signal acts as a frequency modulator.

The simulated FM signal $\Phi_{FM}(t)$, shown in Fig. 5 compared to selected $\delta^{18}O$ time series, successfully reproduces the subtle change in time interval between consecutive ice ages. For times before 1 Ma, the fit deteriorates, because the period of the ice ages becomes dominated by the 41-ky obliquity signal and the eccentricity carriers gradually disappear (Fig. 1, A and B).

How does the climate system frequency-modulate the astronomical forcing? A natural place to search for an analogy is the mechanism of the resonant circuit of an electrical oscillator that generates FM signals as its capacitance or inductance are made to vary (*9*). The simplest analogue paleoclimatic mechanism is a conceptual representation of the climate system as a (potentially) resonant oscillator (*20*), where the linear extent of the ice sheet, L, satisfies an equation of the form

$$d^2L/dt^2 + \Omega^2 L = 0 \qquad (4)$$

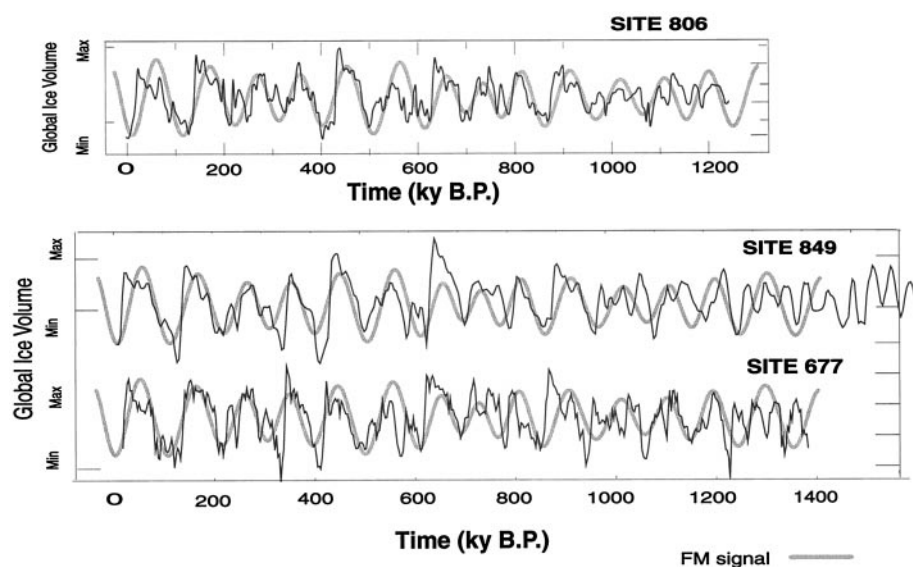where $\Omega = (1/C_L C_T)^{1/2}$ is the natural angular

Fig. 5. Comparison of the FM signal constructed with Eq. 3 and selected $\delta^{18}O$ records. The synthetic FM signal closely reproduces the variable duration of the ice ages. The fit with the data deteriorates for times earlier than ~900 ky B.P., because the 41-ky cycle becomes predominant. The best-fitting signal was obtained by trial-and-error varying the values of the adjustable parameters *a*, *b*, and *c*.

frequency of the climate model, C_T the ocean's thermal overturning time, and C_L the ice cap's relaxation time. There are at least two ways to include external forcing in Eq. 4: with an additive term of the form $F \cos \omega_0 t$, which introduces the possibility of resonance when $\omega_0 \to \Omega$, and/or with a time-varying parameter (parametric excitation), assuming that Ω changes with the dimension of the ice sheet (21) through C_L, which is proportional to a critical dimension of the ice sheet (22).

If C_L is of the form $C_L(1 + \Delta C_L/C_L \cos \omega t)$ where $\Delta C_L \ll C_L$ and ω is the modulating frequency, Eq. 4 becomes

$$\mathrm{d}^2 L/\mathrm{d}t^2 + \Omega^2 \left[1 + 2(\Delta\Omega/\Omega)\cos\omega t\right] L = 0 \tag{5}$$

which is the Mathieu equation (23), whose periodic solutions are frequency-modulated sinusoids (24) of the form

$$L \sim A \sin[\Omega t + (\Delta\Omega/\omega)\sin \omega t + \phi] \tag{6}$$

where A and ϕ are integration constants. The solution to Eq. 6 is of the same form as each of the terms of Eq. 3 used to simulate the $\delta^{18}O$ records. Nonlinear forms of Eq. 5 are known to develop instabilities, bifurcations, and period-doubling cascades into chaos (25).

References and Notes

1. M. Milankovitch, *Canon of Insolation and the Ice-Age Problem*, Royal Serbian Academy Spec. Pub., vol. 132 (Israel Program for Scientific Translations, Jerusalem, 1969).
2. J. D. Hays, J. Imbrie, N. J. Shackelton, *Science* **194**, 1121 (1976).
3. A. Berger and M. F. Loutre, *Quat. Sci. Rev.* **10**, 297 (1991); A. Berger, *Numerical Values of the Elements of the Earth's Orbit from 5,000,000 YBP to 1,000,000 YAP*, Contribution No. 35, Universite Catholique de Louvain, B-1348 Louvain, Belgium (1978).
4. J. Imbrie *et al.*, in *Milankovitch and Climate*, A. L. Berger *et al.*, Eds. (Reidel, Hingham, MA, 1984), pp. 269–305.
5. In order of decreasing spectral amplitude, the main periods in the trigonometric expansion of Earth's orbital eccentricity are, approximately, 413, 95, 125, and 100 ky. The 95 and 413 ky spectral peak amplitudes are nearly equal and about twice as strong as the 125 ky amplitude and four times stronger than the 100 ky amplitude (3).
6. J. Imbrie and J. Z. Imbrie, *Science* **207**, 943 (1980).
7. M. E. Raymo, *Paleoceanography* **12**, 577 (1997).
8. W. H. Berger, M. K. Yasuda, T. Bickert, G. Wefer, T. Takayama, *Geology* **22**, 463 (1994); W. H. Berger, T. Bickert, H. Schmidt, G. Wefer, *Proc. Ocean Drill. Program Part B Sci. Results* **130**, 381 (1993).
9. B. P. Lathi, *Modern Digital and Analog Communication Systems* (Oxford Univ. Press, New York, 1998).
10. The sidebands of a carrier of frequency f_c frequency modulated by a signal of frequency f_m are located at $f_c \pm nf_m$, $n = 1, 2, 3\ldots$. See, for instance, A. Hund, *Frequency Modulation* (McGraw-Hill, New York, 1942).
11. Frequency modulation of the weaker 125 ky eccentricity component essentially reinforces the 95 ky peak and its sidebands, since $1/95 - 1/413 \sim 1/125$. The contribution of the much weaker 100 ky component is noticeable only in some records (Fig. 4A).
12. D. G. Martinson *et al.*, *Quat. Res.* **27**, 1 (1987).
13. Age models for the $\delta^{18}O$ data used in this study are as follows: Site 849 and Site 846 tuning procedures are described in Mix *et al.* (19). For the construction of the untuned records, the following anchor points between depth (revised composite depth in meters, or rmcd) and age were used. Site 846: 0.0 rmcd = 0.00 thousand years before the present (ky B.P.); 65.4 rmcd = 1810 ky B.P. Site 849: 0.0 rmcd = 0.0 ky B.P.; 50.0 rmcd = 1800 ky B.P.; 153.8 rmcd = 5 My B.P. (A. Mix, personal communication). The untuned time scale was then constructed by linear interpolation. Both tuned and raw records are available through anonymous ftp (ftp://oce.orst.edu/DATA/mix). Site 806: The age model for the tuned record of Site 806 is from (8). Site 677: Tuned and depth-dependent data were obtained from the Delphi project Web site (http://delphi.esc.cam.ac.uk/). See also N. J. Shackleton, A. Berger, and W. R. Peltier [*Trans. R. Soc. Edinburgh Earth Sci.* **81**, 251 (1990)]. To construct the untuned record, two anchor points at 0 ky B.P. and at 1200 ky B.P. were transferred from the tuned age model. The untuned time scale was then constructed by linear interpolation.
14. R. A. Muller and G. J. MacDonald, *Science* **277**, 215 (1997).
15. The frequency resolution of a 600 ky window is at best 1/600 ky⁻¹, or 0.00167 cycles/ky, so that the spectrum entirely washes out the gap between the eccentricity's 95-ky carrier and the important 107-ky sideband, separated by a 1/826 = 0.00121 cycles/ky interval, and barely resolves sidebands produced by the 413-ky modulation, separated by multiple integers of 0.00242 cycles/ky. A possible reason for the presence of a strong 100-ky peak in the short window spectra is found in the spectrogram of Fig. 1B, which shows that the highest power in the eccentricity band is associated with a transient event about 400 ka (well within the 0 to 600 ky window), which lasted for about 100 ky and had most of its power between 90 and 110 ky. Low spectral resolution of this transient event can certainly contribute to make the 100-ky peak (14) as prominent as shown in Fig. 3C.
16. Even in tuned spectra, results show [J. Park and K. A. Maasch, *J. Geophys. Res.* **98**, 447 (1993)] that the presence of 95 ky and 125 ky peaks in $\delta^{18}O$ records is unlikely to be an artifact of time scaling techniques, because different time series treated with different tuning schemes contain the two eccentricity peaks prominently, even for times before 1 Ma.
17. Increase in the modulation index ε increases the number of sidebands and hence the bandwidth. Its increase also increases the power of the sidebands relative to the carrier's (Fig. 4).
18. This is because $\sin[\omega_c t + \varepsilon \sin \omega_1 t + \varepsilon' \sin \omega_2 t] \neq \sin[\omega_c t + \varepsilon \sin \omega_1 t] + \sin[\omega_c t + \varepsilon' \sin \omega_2 t]$. An interesting point is then that Eq. 3 represents a climate response that is both linear and nonlinear, since it allows for the linear superposition of the spectra of each individual modulated carrier and its sidebands, while the FM process acting on each carrier is itself nonlinear. In fact, having more than one modulating frequency creates an infinite number of combination tones (this distinguishes FM from AM, or amplitude modulation), and so Eq. 3 predicts that the spectral peak at 107 ky is strong because it is both a sideband of the 95-ky carrier modulated by the 826-ky subharmonic and a nonlinearly produced combination tone, which probably explains why it appears to have its own sidebands (Fig. 4).
19. A. C. Mix *et al.*, *Proc. Ocean Drill. Program Part B Sci. Results* **138**, 371 (1995); A. C. Mix, J. Le, N. J. Shackleton, *ibid.*, p. 839.
20. M. Ghil and S. Childress, *Topics in Geophysical Fluid Dynamics: Atmospheric Dynamics, Dynamo Theory and Climate Dynamics* (Springer-Verlag, Berlin, 1987).
21. The capacitor of a resonating circuit is analogous to the ice sheet in that it stores energy in proportion to its area. An FM signal is created, for instance, by sinusoidally varying the circuit's capacitance.
22. E. Kallén, C. Crafoord, M. Ghil, *J. Atmos. Dyn.* **36**, 2292 (1980).
23. Mathieu's equation is a particular case of Hill's equation, arising in many practical applications and in the theory of astronomical perturbations.
24. L. A. Pipes and L. R. Harvill, *Applied Mathematics for Engineers and Physicists* (McGraw-Hill, New York, 1970).
25. T. Mulin, Ed., *The Nature of Chaos* (Clarendon, Oxford, 1993).
26. L. Hinnov, A. Mix, F. Schmieder, J. Park, and B. Bills provided useful comments, data, and continuous encouragement, for which I will always be grateful. Reaction to a critical anonymous review made this paper publishable. The research was supported in part by grants from NSF, U.S. Department of Energy, and the University of North Carolina Research Council.

The Role of Sub-Milankovitch Climatic Forcing in the Initiation of the Northern Hemisphere Glaciation

K. J. Willis,[1]* A. Kleczkowski,[2]† K. M. Briggs,[2] C. A. Gilligan[2]

Mechanisms responsible for the initiation of major glaciation in the Northern Hemisphere at about 2.75 million years ago are poorly understood. A laminated terrestrial sequence from Pula maar, Hungary, containing about 320,000 years in annual layers between 3.05 and 2.60 million years ago, provides a detailed record of rates of climatic change across this dramatic transition. An analysis of the record implies that climatic variations at sub-Milankovitch frequencies (less than or equal to 15,000 years) were an important driving force during this transitional interval and that, as the threshold was approached, these increased in frequency and amplitude, possibly providing the final trigger for the amplification of Northern Hemisphere ice sheets.

The late Pliocene was a time of major climatic cooling resulting in the growth of large terrestrial ice sheets and the onset of Northern Hemisphere glaciation (NHG) at ~2.75 million years ago (Ma). What triggered this dramatic period of global environmental change has been uncertain (1). Suggestions include climatic change associated with changing continental positions and altered deep ocean circulation (2, 3), a long-term decline in atmospheric CO_2 levels resulting in greenhouse cooling (4), climate change associated with tectonic uplift (5), and decreased rates of sea-floor spreading (6). It has also been suggested that the onset of NHG was